Clinical Application of Quantitative MR Imaging in Nonalcoholic Fatty Liver Disease

Tsujita, Yushi ; Sofue, Keitaro ; Ueshima, Eisuke ; Ueno, Yoshiko ; Hori, Masatoshi ; Murakami, Takamichi

(Citation)
Magnetic Resonance in Medical Sciences,22(4):435-445

(Issue Date)
2023-10-01

(Resource Type)
journal article

(Version)
Version of Record

Magn Reson Med Sci 2023; 22; 435–445
doi:10.2463/mrms.rev.2021-0152 Published Online: May 18, 2022

REVIEW

Clinical Application of Quantitative MR Imaging in Nonalcoholic Fatty Liver Disease

Yushi Tsujita[1], Keitaro Sofue[1*], Eisuke Ueshima[1], Yoshiko Ueno[1], Masatoshi Hori[1], and Takamichi Murakami[1]

Viral hepatitis was previously the most common cause of chronic liver disease. However, in recent years, nonalcoholic fatty liver disease (NAFLD) cases have been increasing, especially in developed countries. NAFLD is histologically characterized by fat, fibrosis, and inflammation in the liver, eventually leading to cirrhosis and hepatocellular carcinoma. Although biopsy is the gold standard for the assessment of the liver parenchyma, quantitative evaluation methods, such as ultrasound, CT, and MRI, have been reported to have good diagnostic performances. The quantification of liver fat, fibrosis, and inflammation is expected to be clinically useful in terms of the prognosis, early intervention, and treatment response for the management of NAFLD. The aim of this review was to discuss the basics and prospects of MRI-based tissue quantifications of the liver, mainly focusing on proton density fat fraction for the quantification of fat deposition, MR elastography for the quantification of fibrosis, and multifrequency MR elastography for the evaluation of inflammation.

Keywords: *fat, fibrosis, inflammation, magnetic resonance imaging, nonalcoholic fatty liver disease*

Introduction

There are many causes of diffuse liver disease, such as viral hepatitis, autoimmune hepatitis, hemosiderosis, alcohol, and fatty liver.[1] Chronic and persistent inflammatory changes in the liver cause repetitive destruction and regeneration of the liver parenchyma, which eventually lead to fibrosis, cirrhosis, and the development of hepatocellular carcinoma.[2–4] In the past, hepatitis viruses, such as hepatitis viruses B and C, were the leading causes of chronic liver diseases. However, with the development of treatment methods, the number of patients with chronic liver diseases caused by hepatitis viruses has been decreasing in developed countries, such as Western countries and Japan.[5,6] The proportion of non-B and non-C chronic liver diseases have been increasing because of the globally increasing prevalence of nonalcoholic fatty liver (NAFL) disease (NAFLD), which one in four adults suffer from.[7,8] NAFLD encompasses a histological spectrum ranging from NAFL, which is characterized by minor fat deposition without inflammation, to nonalcoholic steatohepatitis (NASH), which manifests as inflammation and ballooning, with or without fibrosis.[9] It is estimated that 25%–44% of patients with NAFL will develop NASH, 5%–38% of whom will progress to cirrhosis, and that within eight years, 2.4%–12.8% of patients with NAFLD-related cirrhosis will develop hepatocellular carcinoma.[9–13] It is of utmost importance to prevent the progression to NASH and to early detect the high-risk groups. Regarding the diagnosis of NAFLD, when fatty liver or abnormal liver function is found, the hepatitis virus or autoimmune diseases should be first ruled out. By examining the history of alcoholism, alcoholic liver disease can also be excluded and NAFLD can be considered. Scoring systems, such as the fibrosis-4 (FIB-4) index and the NAFLD fibrosis score, are used to differentiate between NAFL and NASH, but they are not absolutely accurate.[14,15] Thus, liver biopsy is used to confirm the diagnosis of NASH.[16]

The pathology of NASH is characterized by inflammation of the hepatic parenchyma, ballooning of hepatocytes, and macrovesicular fatty liver; as the disease progresses, fibrosis develops around the central veins.[17] The NAFL Activity Score system scores the degree of fat deposition, lobular inflammation, and ballooning to diagnose NASH and, along with the stage of fibrosis, determines the degree of disease progression.[18] Although liver biopsy is the gold standard for NASH diagnosis, it is not practical to perform liver biopsy in all patients with NAFLD.[16] Liver biopsy can

[1]Department of Radiology, Kobe University Graduate School of Medicine, Kobe, Hyogo, Japan

*Corresponding author: Department of Radiology, Kobe University Graduate School of Medicine, 7-5-2, Kusunoki-cho, Chuo-ku, Kobe, Hyogo 650-0017, Japan. Phone: +81-78-382-6104, Fax: +81-78-382-6129, E-mail: keitarosofue@gmail.com

Received: November 29, 2021 | Accepted: March 23, 2022

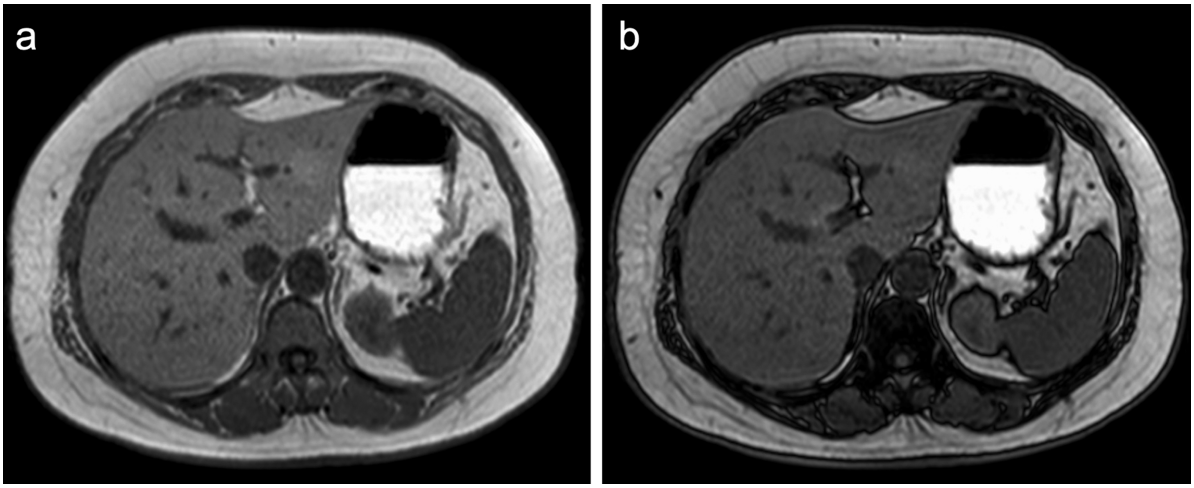

Fig. 1 In the two-point Dixon method, in-phase and opposed-phase images can be obtained using the chemical-shift difference between water and fat protons. This is an example of a patient with nonalcoholic steatohepatitis. The signal intensity of the liver parenchyma decreases from the in-phase (**a**) to the opposed-phase image (**b**).

yield only 1/20000 to 1/50000 of the total liver volume, and there is a risk of sampling error. It is highly invasive and causes serious complications in approximately 0.5% of patients, and there is variability in the diagnosis even among experienced pathologists.[19–22]

To compensate for the disadvantages of liver biopsy, noninvasive imaging methods, such as ultrasound (US), CT, and MRI, have been developed. In this review, we discuss the basics and prospects of MRI-based tissue quantifications of the liver, mainly focusing on the quantitative assessment of fat deposition, fibrosis, and inflammation.

Quantification of Steatosis

Pathophysiology

Fatty liver is characterized by the excessive accumulation of triglycerides in the cells of the liver. This is one of the pathological features of NAFLD, but this can also be caused by other viral liver diseases, alcoholic liver disease, lipodystrophy, glycogenosis, and fatty drugs.[23,24] Normally, fat in the liver serves as energy (triglycerides and cholesterol esters) storage when there is excess energy, releasing them during extended fasting.[25] When lipid homeostasis becomes imbalanced due to abnormal conditions, such as metabolic diseases or obesity, excess triglycerides accumulate in the hepatocytes. Some cases of NAFLD progress to NASH, which can lead to cirrhosis and liver cancer; thus, an early diagnosis is of great clinical significance.[2,4,24]

Chemical-shift-based proton density fat-fraction

The Dixon method is widely known as a method for fat quantification (Fig. 1). In the usual two-point Dixon method, in-phase and opposed-phase images are taken using the chemical-shift difference between water and fat protons, and the fat fraction can be calculated from the obtained signal intensity ($F = [I - O]/2$, $W = [I + O]/2$, Fat fraction = $F/W + F$; F, W, I, O: signal intensity of fat, water, in-phase, and opposed-phase, respectively). Some reports found that fat quantification obtained by two-point Dixon method also correlates well with histopathological fat deposition.[26,27] However, this method has several problems. Triglycerides, which are the fat in the body, have six peaks on the MR spectroscopy (MRS), but the two-point Dixon method assumes only the fat signal of beta-carboxyl methylene, which peaks at 1.3 ppm.[28,29] It accounts for only approximately 70% of the total body fat, thus underestimating the fat fraction. In addition, diffuse liver disease causes intrahepatic iron deposition, which leads to the underestimation of the signal due to T2* shortening and overestimation of the signal due to the effect of the T1 value, resulting in inaccurate fat quantification.[30,31] A fat fraction map using the Dixon method with multi-echo can overcome these weaknesses. Increasing the number of echo samples allows for multi-peak fat quantification and T2* value correction, and reducing the flip angle minimizes the effect of the T1 value.[32,33] The fat quantification image adjusted for these confounding factors is called proton density fat fraction (PDFF) map (Figs. 2 and 3).

PDFF measures the proportion of proton components of fat molecules and is not identical to the pathologically defined lipid droplets in hepatocytes. It has been reported that PDFF threshold of 6.4% is consistent with the fatty liver criteria in pathology.[34,35] Tang et al. proposed the PDFF cut-off to classify steatosis grades, with high-specificity cut-offs of about ≥ 6.4%, ≥ 17.4%, and ≥ 22.1% corresponding to steatosis grades of ≥ 1, ≥ 2, and 3, respectively.[34] PDFF has been proven to be highly accurate and reproducible in phantom experiments and clinical cases, and is optimal as an imaging biomarker since it yields minimal error in MR

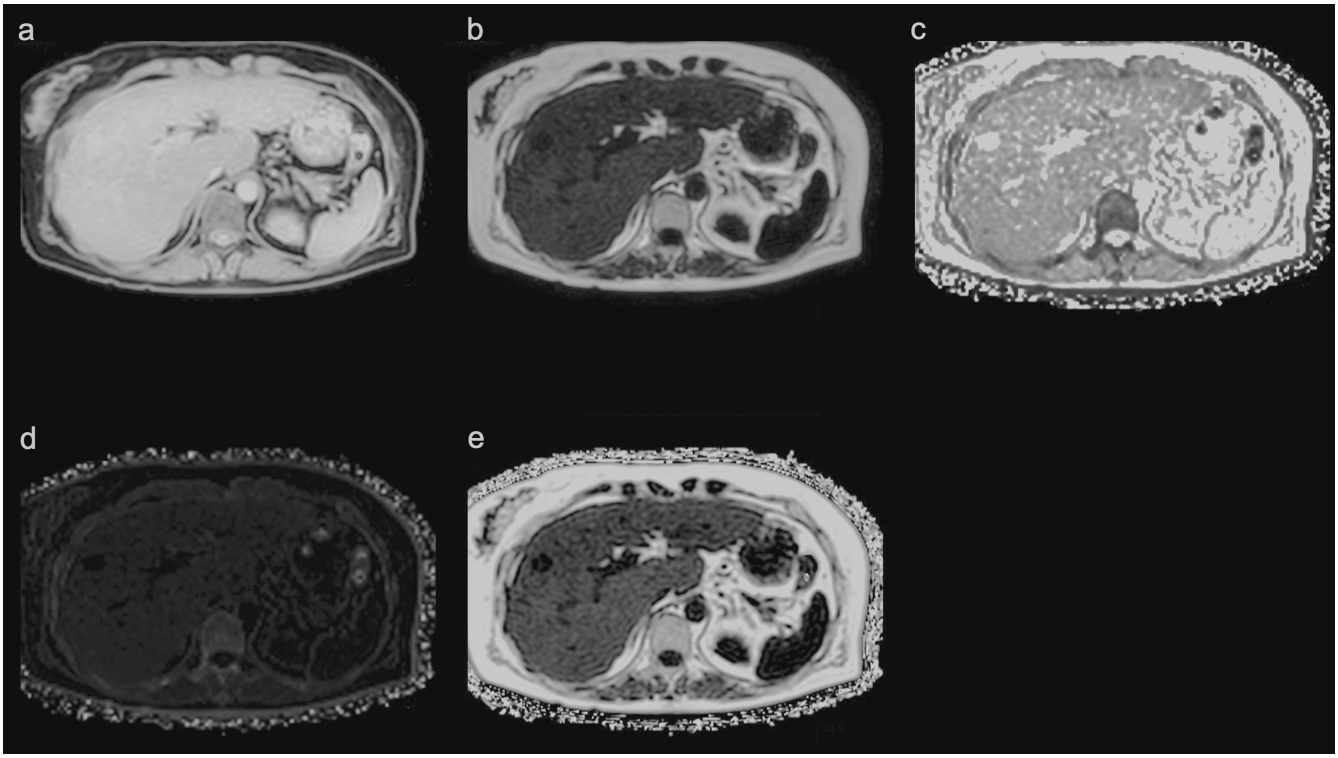

Fig. 2 In the multi-echo Dixon method, five images, a water image (**a**), fat image (**b**), T2* map (**c**), R2* map (**d**), and PDFF map (**e**) can be obtained with a single scan. PDFF (%) is obtained by setting the ROI on the PDFF map. PDFF, proton density fat fraction.

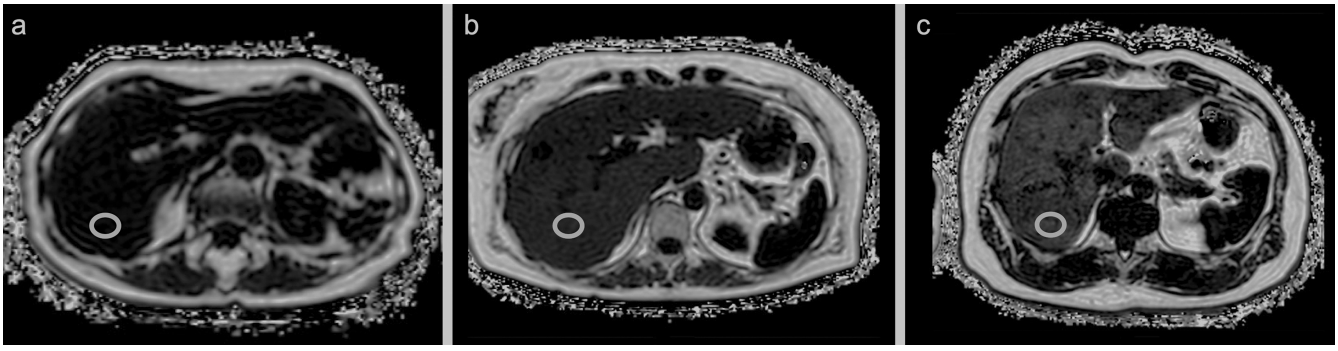

Fig. 3 PDFF maps of three patients. The entire liver was evaluated in only a single 16s breath-hold. ROIs were placed in the posterior segment. PDFF values of the first patient showed minimal fat deposition in the liver (normal, < 6%) (**a**). PDFF values of the second and third patients revealed medium and high degrees of liver fat deposition (10.5% and 15.1%), respectively (**b** and **c**). PDFF, proton density fat fraction.

models and magnetic field strength.[36,37] In addition, while fat deposition in the liver is often heterogenous, the ability to evaluate the entire liver provides clinical value superior to that of biopsy.[38,39] This imaging method also simultaneously produces the R2* map, which is useful for the assessment of iron deposition.[40,41] Iron is an important micronutrient in the oxygen transport system of hemoglobin, but excessive iron deposition in the liver can cause oxidative stress that leads to mitochondrial dysfunction and deoxyribonucleic acid (DNA) damage, resulting in hepatocellular injury, liver fibrosis, and cirrhosis.[42,43] Meanwhile, hereditary hemochromatosis, long-term blood transfusion, and hematological diseases that cause hemolytic anemia (e.g., thalassemia and sickle cell disease) are common causes of iron deposition and diffuse liver diseases, such as NAFLD and alcoholic and viral hepatitis.[44] It is widely known that the R2* value correlates well with the amount of liver iron.[40,41] The cut-off value for R2* values in iron deposition was reported to be 60 s^{-1} by 1.5 T MRI and 126 S^{-1} by 3.0 T MRI.[40] Bashir et al. reported that in patients with NAFLD, the most influential

factor on hepatic R2* values was hepatic fat deposition as measured by PDFF.[45] This study showed that R2* values may not accurately reflect hepatic iron deposition in cases of excessive fat deposition in the liver.

Limitations of the PDFF

Although PDFF is an established imaging technique for the quantification of liver fat, it requires a long breath-hold because of 3D Cartesian sampling. In patients with difficulty in breath-holding, coherent aliasing artifacts make fat quantification inaccurate. Imaging with 3D stack of radial sampling under free breathing conditions can significantly reduce motion artifacts compared with conventional methods. It has been reported to be as accurate as conventional PDFF and MRS in phantoms and healthy volunteers and to improve the image quality of PDFF in infants with difficulty in breath-holding.[46,47] Another countermeasure for the long breath-holding time can be compressed sensing (CS).[48,49] This minimizes compressible image data using incoherent undersampling and an iterative reconstruction algorithm to shorten scan time and minimize motion effects.[50] In a qualitative and quantitative study comparing PDFF with four levels of CS factors and conventional PDFF, it was reported that the same accuracy was achieved even when the imaging time was shortened to one-fourth of the original time.[49]

Another weakness of PDFF is that T2* correction by the fitting model becomes inaccurate due to premature T2* shortening in cases of severe iron deposition. Although ultrashort TE is expected to be used to acquire signals in a shorter time than T2* shortening, some studies have suggested that there is a short T2* signal in the liver, and that the PDFF bias is larger in ultrashort TE than in short TE, which had to be corrected by excluding short echoes below 1 ms.[51,52] On the other hand, the good accuracy of PDFF has been reported in cases with severe T2* shortening, such as before and after superparamagnetic iron oxide administration and in patients with hemochromatosis.[53,54] The R2* values in diffuse liver diseases, such as NAFLD, alcoholic liver disease, and viral hepatitis, are much lower than those in the aforementioned severe iron deposition cases, and the effect of T2* shortening may not be significant.

Other imaging techniques

MRS is a measure for hepatic fat quantification by MRI, and the diagnostic performance of PDFF has been reported to be almost equivalent to that of MRS.[31,55] However, MRS is limited in scan coverage and usually evaluates only a single voxel. MRS is considered inferior to PDFF because fat deposition in the liver is often heterogeneous, overall evaluation is important, and reproducibility is necessary for the evaluation of treatment effects.[29,37] For these reasons, MRS has been replaced by PDFF.

In US examination, Fibroscan (approved by the Food and Drug Administration in 2013; EchosensTM, Paris, France), equipped with the controlled attenuation parameter (CAP) function, can measure the US attenuation of the generated shear waves and estimate the fat deposition. However, in comparative studies between PDFF and CAP, PDFF was superior in diagnosing mild, moderate, and severe fatty liver.[56,57] The considered reason was that PDFF directly quantifies the fat molecule proton ratio, while CAP is an indirect semi-quantitative evaluation that utilizes the correlation between US attenuation and the degree of liver fat.

Dual-energy CT (DECT) is a technique that uses two different energies for imaging. DECT can determine the concentration of constituent materials in a mixture with a process known as material decomposition.[58] Fat, iron, and healthy liver tissue have adequately different mass attenuation coefficients with one another, which allow the direct quantification of liver fat and iron with material decomposition algorithms. It was reported that, in grading hepatic steatosis, DECT had comparable diagnostic performance to MRS.[59]

Quantification of Fibrosis

Pathophysiology

Liver fibrosis in chronic liver diseases is caused by the repeated inflammation, destruction, and regeneration of tissues over many years due to chronic liver diseases, resulting in the activation of stellate cells, proliferation of fibroblasts and myofibroblasts, and excessive deposition of collagen as an extracellular matrix.[60] When fibrosis progresses and the regenerative capacity decreases, this leads to cirrhosis. Since hepatic fibrosis is the most significant prognostic factor in chronic liver diseases, early diagnosis and treatment of the causative disease leads to a better patient outcome.[61,62]

MR elastography

MR elastography (MRE) applies vibrations from outside of the body, transmits propagate elastic waves through the tissue, and estimates the tissue stiffness by measuring the wavelength (Fig. 4).[63,64] With the assumption that the liver is an elastic material, the elastic modulus, an index of stiffness, can be expressed using the following formula:[63]

$v^2 = \mu/\rho$ (v: elastic wave velocity, μ: shear modulus, ρ: material density)

The density of the liver is almost 1 g/cm^3,[65] and the elastic wave velocity is the multiplication of the frequency *f* and the wavelength λ. The elastic modulus could be obtained by vibrating the liver at a fixed vibration frequency and measuring the wavelength. The principle of MRE is that the rotational phases of protons are aligned to a homogeneous material, but by shifting the rotational phase, the physical vibrations transmitting in the liver can be visualized on phase images. The phase images are processed by an algorithm to obtain an elastogram. When comparing the wave images taken in normal and cirrhotic livers, the wavelength is longer

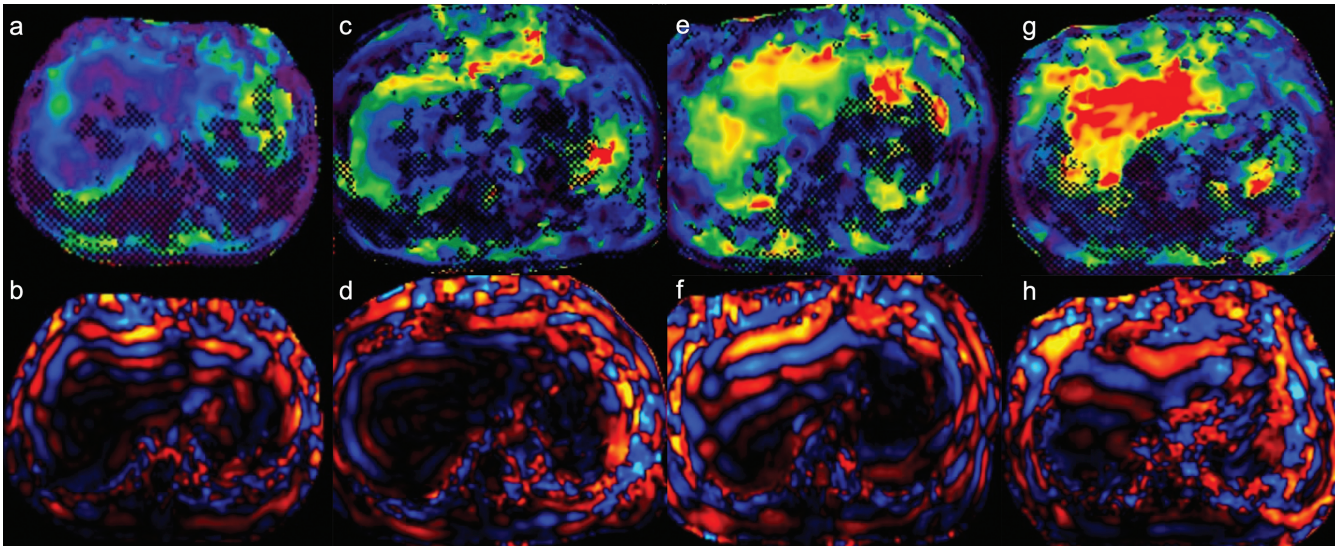

Fig. 4 MR elastograms and wave images of four patients. The modulus of elasticity increased with the stage of fibrosis. The stiffness values of the liver were as follows: 2.43 kPa in the patient with F1 (biopsy specimen scored using New Inuyama Classification) (**a** and **b**), 2.97 kPa in F2 (**c** and **d**), 5.65 kPa in F3 (**e** and **f**), and 9.24 kPa in F4 (**g** and **h**).

and the elastic waves transmit faster in the latter. MRE could be easily added to conventional liver MRI protocols to evaluate the stiffness of the entire liver. It is not affected by ascites, obesity, fatty liver, or intravenous contrast administration, resulting in high reproducibility.[66,67] Multiple studies comparing histological fibrosis scores and elastic moduli measured using MRE in patients with chronic liver disease have reported a good correlation, with elastic moduli increasing as fibrosis progressed.[68–70] According to a multicenter study, the cut-off value of MRE for liver fibrosis in patients with various etiology of chronic liver diseases was reported as follows, all of which showed high diagnostic performance:

F1: 3.45 kPa (AUC: 0.84 [95% CI: 0.76–0.92]), F2: 3.66 kPa (AUC: 0.88 [95% CI: 0.84–0.91]), F3: 4.11 kPa (AUC: 0.93 [95% CI: 0.90–0.95]), F4: 4.71 kPa (AUC: 0.92 [95% CI: 0.90–0.94])[71]

Consensus profile by quantitative imaging biomarker alliance suggested that ROIs should be drawn manually in the largest possible area of liver parenchyma in which coherent shear waves are visible while excluding major blood vessels seen on the MRE magnitude images.[72] In addition, various methods of ROIs placement have been reported, with the placement of a small round ROI in each segment (four segments or eight segments), the largest possible ROI in the entire liver or right lobe, a small ROI in the anterior segment, and such others.[73–75] Lee et al. reported that placing a round ROI in each segment and a large ROI in the entire liver was significantly more reliable than placing a small ROI in the anterior segment.[73] Since liver fibrosis has been reported to be highly variable among the segments, Toguchi et al. tested a method of averaging liver stiffness obtained from small ROIs placed in the right lobe of several slices.[76] They speculated that measuring liver stiffness in the same segment as the biopsy site would provide a better correlation with histological fibrosis. The study showed a significantly better correlation with the stage of histological fibrosis compared to a large freehand ROI placed in the right lobe.

Limitations of MRE

Conventional 2D MRE are sensitized to detect motion in a single plane and to work on the principle that shear waves transmit through the axial plane of acquisition. This hypothesis does not apply for regions of the liver close to the dome or below or far from the passive driver. In such regions, the waves may be transmitting at an oblique angle to the axial direction, and the wavelengths of shear wave may be overestimated. The 3D MRE is sensitized to detect motion in all three planes and can correct for wave obliquity.[77] The 3D MRE, usually spin-echo based, could evaluate the entire liver with a few breath-holds. This technique corrects for wave skewing and has a higher diagnostic performance than 2D MRE.[78]

Technical failures account for less than 5% of examinations and are most commonly caused by a reduced SNR due to iron overload in the liver.[71] The pulse sequence typically used in MRE is the gradient-echo technique, which requires a long TE and is susceptible to T2* shortening due to iron deposition. In addition, it has been reported that this phenomenon is more likely to occur in 3T MRI scanners.[79] Spin echo-echo planar imaging (SE-EPI) was recently developed as a pulse sequence that can be used in 3T MRE.[80] SE-EPI has advantages, such as low sensitivity to the attenuation of the transverse relaxation signal and wide coverage since

multiple slices can be acquired with a single breath-hold. It is expected to reduce the overall technical failure rate.[79,80]

Other imaging techniques

The US transient elastography can also quantify liver stiffness by measuring the velocity of shear waves generated by the probe. In comparison between MRE and US elastography, MRE was slightly superior in terms of the diagnostic performance in all fibrosis stages.[81] Another advantage is that MRE is not dependent on radiographers and has greater reproducibility.[75,82–84]

Other imaging techniques using MRI that show promise for the evaluation of hepatic fibrosis include diffusion weighted imaging (DWI), intravoxel incoherent motion (IVIM), T1 mapping, and T1ρ mapping. DWI is a technique for imaging molecular motion and diffusivity. The pathological structure of liver tissue changes due to fibrosis, and diffusivity is greatly affected by the degree of fibrosis.[85,86] Although a large number of studies have shown that liver fibrosis and apparent diffusion coefficient (ADC) values are inversely correlated, a recent meta-analysis reported that DWI also showed a good diagnostic performance for histological fibrosis staging but was inferior to MRE.[85,87] Since the liver is a highly vascularized organ, perfusion has a significant impact on diffusivity. IVIM, a biexponential model of DWI introduced by Le Bihan et al., can evaluate capillary microcirculation and water diffusion separately by analyzing the signal attenuation of multi-b-value DWI.[88] However, there are some reports that MRE has a higher diagnostic performance than IVIM.[89,90] On the other hand, diffusion-weighted-based virtual elastography has recently been developed and reported to have comparable diagnostic performance to MRE.[91,92] T1 and T1ρ are sensitive to low-frequency exchange interactions between water molecules and the large, slow-tumbling macromolecules, such as collagen, and can be used biomarkers of liver cirrhosis. Although it is not currently an established imaging method, some reports have shown that T1 and T1ρ values strongly correlated with US elastography, and further studies on this topic are expected.[93,94] The liver stiffness measurement obtained with standard clinical MRE sequences represents the apparent elasticity of the liver parenchyma and cannot be distinguished from that due to inflammation, congestion, or increased vascular pressure. A more accurate quantification of liver fibrosis is expected by separating fibrosis and inflammation, as described in the next chapter.

Quantification of Inflammation

Pathophysiology

Fatty deposits in the liver are the cause of NASH, but the presence of fatty deposits does not necessarily lead to NASH. The two-hit theory and multiple parallel hit theory are known as hypotheses of the process from NAFL to NASH.[95,96] In the two-hit theory proposed by Day et al., background factors, such as overnutrition and metabolic syndrome-induced fat deposition in the liver, lead to the development of NAFL.[95] This is followed by secondary stresses, such as oxidative stress, inflammatory cytokines, and endotoxins derived from intestinal bacteria, leading to inflammation of the liver and progression to NASH. Recently, interactions with extrahepatic organs, such as adipose tissue and the intestinal tract, have been reported to be a factor in the development of NASH.[97] It is important to accurately assess persistent inflammation in the liver to detect the early development of NASH.

Multifrequency MR elastography

MRE measures the elastic modulus of the liver to estimate fibrosis. It was also found via MRE that inflammation also increases the elastic modulus. In the presence of inflammation, the elastic modulus shows a high value due to increased intra-tissue pressure caused by increased regional blood flow, congestive edema, and inflammatory cell infiltration.[98] Ichikawa et al. reported that, in patients with chronic liver disease, the presence of inflammation increases the elastic modulus at all fibrosis stages.[99] The elastic modulus of cases with low fibrosis stage and high activity grade was similar to those with high fibrosis and low activity, indicating that the degree of inflammation had a significant effect on the elastic modulus. Liver stiffness on MRE is calculated by assuming that the liver tissue is a homogeneous isotoropic elastic body. However, liver tissue is generally composed of a viscoelastic body, and elastography, by using shear wave propagation, is needed to be determined as viscoelasticity. In the Voigt model, the elastic modulus can be expressed as a complex modulus and is calculated from the elastic and viscous moduli, while conventional single frequency MRE is not capable of evaluating the elastic and viscous tissues separately.[100] In reality, biological soft tissues are viscoelastic, with a mixture of elastic and viscous materials. The stiffness values on MRE by using inversion algorithm are composed of storage modulus (elastic property) and shear loss modulus (viscous property). The velocity and attenuation of shear waves in the viscous tissues are greater at higher vibration frequencies due to the diffusion of elastic waves in the viscous media, while elasticity in the elastic tissues is largely independent of frequency. Thus, higher vibration frequency on MRE can emphasize the viscous property compared with the elastic property.[101,102] According to this nature, multifrequency MRE with multiple vibration frequencies may be able to evaluate liver inflammation separately from fibrosis (Fig. 5). In a study using an animal model, complex modulus and damping ratio (viscosity to elasticity) obtained from multifrequency MRE correlated with fibrosis and inflammation, respectively.[103] Sofue et al. measured the elastic moduli of 30 patients with various chronic liver diseases, including NASH, using MRE at vibration frequencies of 60 Hz and 80 Hz.[104] They found that the elastic moduli imaged at 80 Hz were always higher than those at 60 Hz and that the

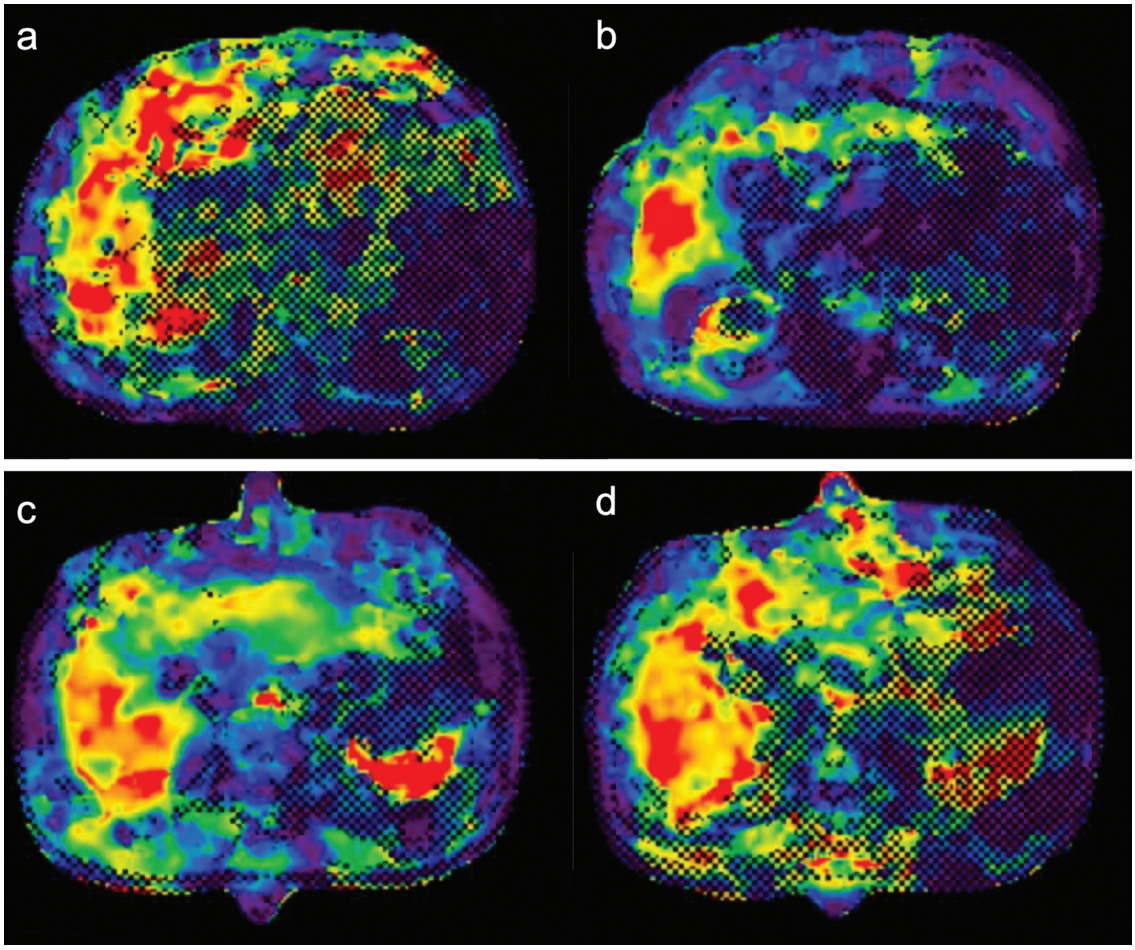

Fig. 5 MR elastograms at 60-Hz and 80-Hz vibration frequencies of two patients. The first patient, a 67-year-old man with chronic hepatitis C, fibrosis stage F3, and necroinflammation grade A1, had stiffness values in MR elastograms at 60 Hz and 80 Hz of 7.82 kPa and 8.23 kPa, respectively (**a** and **b**). The ΔG value was calculated as 0.41 kPa. The second patient, an 82-year-old man with chronic hepatitis C, fibrosis stage F3, and necroinflammation grade A2, had stiffness values at 60 Hz and 80 Hz of 5.40 kPa and 6.78 kPa, respectively (**c** and **d**). The ΔG value was calculated as 1.38 kPa.

difference, ΔG, correlated strongly with the histological activity grade. The modulus at 80 Hz correlated more strongly with the activity grade than the modulus at 60 Hz, and the correlation became even stronger when ΔG was taken into account. Thus, by changing the vibration frequency, the effect of viscosity on the elastic modulus can be captured, which is expected to be useful for diagnosing inflammation. Multiparametric 3D MRE can also provide basic viscoelastic modeling of tissues and separate the complex shear moduli into elastic and viscous components. A recent study found that among several parameters obtained using 3D MRE in patients with chronic hepatitis B and C, the damping ratio correlated well with the activity score in mild liver fibrosis patients, suggesting the possibility of the sensitive detection of early liver inflammation.[105] However, when liver fibrosis progresses, the damping ratio decreases and loses its ability to measure early necroinflammation. Currently, the MRE technics, including 3D MRE, SE-EPI, and multifrequency MRE, described in this paper, are not clinically available.

Other imaging techniques

The random movement of water molecules could be assessed with DWI. ADC, a marker of diffusion, has been reported to be decreased in inflammatory liver tissue, but the results have not been sufficient to quantify inflammation of the liver.[106,107] ADC is affected by perfusion in addition to diffusion effects, and the two effects may be offset or confounded. IVIM is a more advanced method of analyzing diffusion signals and can separate diffusion effects from perfusion effects. Perfusion-related parameters, such as perfusion rate and pseudo-diffusion coefficient, may reflect microvascular changes associated with inflammation. The diagnostic performance of these parameters in noninvasively

detecting inflammation is limited and has been reported to have little or no correlation with inflammation.[108,109] Some reports used T1 mapping and T2 mapping to assess inflammation and have found some correlation, while others have reported that radiomic models based on T1 values corrected for T2* or T2 weighted sequences have shown promising results.[110–112]

Conclusion

In the diagnosis and treatment of NAFLD, it is important to evaluate the presence of fatty deposits, fibrosis, and inflammation in the liver, and to compare and evaluate these factors cross-sectionally during the follow-up and therapeutic monitoring period. Chemical-shift-based PDFF can reliably quantify steatosis of the liver, and MRE can accurately estimate liver fibrosis. In addition, recent papers support adoption of MRI to estimate inflammation of the liver by using multifrequency MRE and other techniques. Quantitative MRI can be expected to play a pivotal role in screening, diagnosis, and treatment monitoring for the assessment of NAFLD by evaluating pathological change in the liver comprehensively and noninvasively.

Acknowledgments

We would like to thank Messrs. Onoda and Morimoto (Kanazawa University Hospital Radiology Division) for providing the figures and Editage (www. editage. com) for English language editing.

Conflicts of Interest

The authors have no conflicts of interest directly relevant to the content of this article.

References

1. Sepanlou SG, Safiri S, Bisignano C, et al. The global, regional, and national burden of cirrhosis by cause in 195 countries and territories, 1990-2017: a systematic analysis for the Global Burden of Disease Study 2017. Lancet Gastroenterol Hepatol 2020; 5:245–266.
2. Byrne CD, Targher G. NAFLD: a multisystem disease. J Hepatol 2015; 62(Suppl):S47–S64.
3. Gluchowski NL, Becuwe M, Walther TC, Farese RV Jr. Lipid droplets and liver disease: from basic biology to clinical implications. Nat Rev Gastroenterol Hepatol 2017; 14:343–355.
4. Nassir F, Rector RS, Hammoud GM, Ibdah JA. Pathogenesis and prevention of hepatic steatosis. Gastroenterol Hepatol (N Y) 2015; 11:167–175.
5. Sagnelli E, Macera M, Russo A, Coppola N, Sagnelli C. Epidemiological and etiological variations in hepatocellular carcinoma. Infection 2020; 48:7–17.
6. Tanaka J, Akita T, Ko K, Miura Y, Satake M. Countermeasures against viral hepatitis B and C in Japan: An epidemiological point of view. Hepatol Res 2019; 49:990–1002.
7. Wong SW, Ting YW, Chan WK. Epidemiology of non-alcoholic fatty liver disease-related hepatocellular carcinoma and its implications. JGH Open. 2018; 2:235–241.
8. Younossi Z, Tacke F, Arrese M, et al. Global perspectives on nonalcoholic fatty liver disease and nonalcoholic steatohepatitis. Hepatology 2019; 69:2672–2682.
9. Calzadilla Bertot L, Adams LA. The natural course of non-alcoholic fatty liver disease. Int J Mol Sci 2016; 17:774.
10. McPherson S, Hardy T, Henderson E, Burt AD, Day CP, Anstee QM. Evidence of NAFLD progression from steatosis to fibrosing-steatohepatitis using paired biopsies: implications for prognosis and clinical management. J Hepatol 2015; 62:1148–1155.
11. Pais R, Charlotte F, Fedchuk L, et al. A systematic review of follow-up biopsies reveals disease progression in patients with non-alcoholic fatty liver. J Hepatol 2013; 59:550–556.
12. Singh S, Allen AM, Wang Z, Prokop LJ, Murad MH, Loomba R. Fibrosis progression in nonalcoholic fatty liver vs nonalcoholic steatohepatitis: a systematic review and meta-analysis of paired-biopsy studies. Clin Gastroenterol Hepatol. 2015; 13:643–654.e1–9; quiz e39–40.
13. Wong VW, Wong GL, Choi PC, et al. Disease progression of non-alcoholic fatty liver disease: a prospective study with paired liver biopsies at 3 years. Gut 2010; 59:969–974.
14. Angulo P, Hui JM, Marchesini G, et al. The NAFLD fibrosis score: a noninvasive system that identifies liver fibrosis in patients with NAFLD. Hepatology 2007; 45:846–854.
15. Balakrishnan M, Loomba R. The role of noninvasive tests for differentiating NASH from NAFL and diagnosing advanced fibrosis among patients with NAFLD. J Clin Gastroenterol 2020; 54:107–113.
16. Younossi ZM, Loomba R, Anstee QM, et al. Diagnostic modalities for nonalcoholic fatty liver disease, nonalcoholic steatohepatitis, and associated fibrosis. Hepatology 2018; 68:349–360.
17. Day CP, Saksena S. Non-alcoholic steatohepatitis: definitions and pathogenesis. J Gastroenterol Hepatol 2002; 17(Suppl 3): S377–S384.
18. Kleiner DE, Brunt EM, Van Natta M, et al. Design and validation of a histological scoring system for nonalcoholic fatty liver disease. Hepatology 2005; 41:1313–1321.
19. Boyd A, Cain O, Chauhan A, Webb GJ. Medical liver biopsy: background, indications, procedure and histopathology. Frontline Gastroenterol 2020; 11:40–47.
20. Jayakumar S, Middleton MS, Lawitz EJ, et al. Longitudinal correlations between MRE, MRI-PDFF, and liver histology in patients with non-alcoholic steatohepatitis: Analysis of data from a phase II trial of selonsertib. J Hepatol 2019; 70:133–141.
21. Ratziu V, Charlotte F, Heurtier A, et al. Sampling variability of liver biopsy in nonalcoholic fatty liver disease. Gastroenterology 2005; 128:1898–1906.
22. Tapper EB, Lok ASF. Use of liver imaging and biopsy in clinical practice. N Engl J Med 2017; 377:756–768.

23. Adinolfi LE, Gambardella M, Andreana A, Tripodi MF, Utili R, Ruggiero G. Steatosis accelerates the progression of liver damage of chronic hepatitis C patients and correlates with specific HCV genotype and visceral obesity. Hepatology 2001; 33:1358–1364.
24. Chalasani N, Younossi Z, Lavine JE, et al. The diagnosis and management of nonalcoholic fatty liver disease: Practice guidance from the American Association for the Study of Liver Diseases. Hepatology 2018; 67:328–357.
25. Rui L. Energy metabolism in the liver. Compr Physiol 2014; 4:177–197.
26. Fischer MA, Nanz D, Reiner CS, et al. Diagnostic performance and accuracy of 3-D spoiled gradient-dual-echo MRI with water- and fat-signal separation in liver-fat quantification: comparison to liver biopsy. Invest Radiol 2010; 45:465–470.
27. Hayashi T, Saitoh S, Takahashi J, et al. Hepatic fat quantification using the two-point Dixon method and fat color maps based on non-alcoholic fatty liver disease activity score. Hepatol Res 2017; 47:455–464.
28. Hamilton G, Yokoo T, Bydder M, et al. In vivo characterization of the liver fat ^{1}H MR spectrum. NMR Biomed 2011; 24:784–790.
29. Reeder SB, Cruite I, Hamilton G, Sirlin CB. Quantitative assessment of liver fat with magnetic resonance imaging and spectroscopy. J Magn Reson Imaging 2011; 34:729–749.
30. Lee SS, Lee Y, Kim N, et al. Hepatic fat quantification using chemical shift MR imaging and MR spectroscopy in the presence of hepatic iron deposition: validation in phantoms and in patients with chronic liver disease. J Magn Reson Imaging 2011; 33:1390–1398.
31. Meisamy S, Hines CD, Hamilton G, et al. Quantification of hepatic steatosis with T1-independent, T2-corrected MR imaging with spectral modeling of fat: blinded comparison with MR spectroscopy. Radiology 2011; 258:767–775.
32. Hernando D, Sharma SD, Kramer H, Reeder SB. On the confounding effect of temperature on chemical shift-encoded fat quantification. Magn Reson Med 2014; 72:464–470.
33. Reeder SB, Robson PM, Yu H, et al. Quantification of hepatic steatosis with MRI: the effects of accurate fat spectral modeling. J Magn Reson Imaging 2009; 29:1332–1339.
34. Tang A, Desai A, Hamilton G, et al. Accuracy of MR imaging-estimated proton density fat fraction for classification of dichotomized histologic steatosis grades in nonalcoholic fatty liver disease. Radiology 2015; 274:416–425.
35. Tang A, Tan J, Sun M, et al. Nonalcoholic fatty liver disease: MR imaging of liver proton density fat fraction to assess hepatic steatosis. Radiology 2013; 267:422–431.
36. Qu Y, Li M, Hamilton G, Zhang YN, Song B. Diagnostic accuracy of hepatic proton density fat fraction measured by magnetic resonance imaging for the evaluation of liver steatosis with histology as reference standard: a meta-analysis. Eur Radiol 2019; 29:5180–5189.
37. Yokoo T, Serai SD, Pirasteh A, et al. Linearity, bias, and precision of hepatic proton density fat fraction measurements by using MR imaging: A meta-analysis. Radiology 2018; 286:486–498.
38. Bannas P, Kramer H, Hernando D, et al. Quantitative magnetic resonance imaging of hepatic steatosis: Validation in ex vivo human livers. Hepatology 2015; 62:1444–1455.
39. Sofue K, Mileto A, Dale BM, Zhong X, Bashir MR. Interexamination repeatability and spatial heterogeneity of liver iron and fat quantification using MRI-based multistep adaptive fitting algorithm. J Magn Reson Imaging 2015; 42:1281–1290.
40. Labranche R, Gilbert G, Cerny M, et al. Liver iron quantification with MR imaging: A primer for radiologists. Radiographics 2018; 38:392–412.
41. Wood JC. Guidelines for quantifying iron overload. Hematology (Am Soc Hematol Educ Program) 2014; 2014:210–215.
42. Anderson ER, Shah YM. Iron homeostasis in the liver. Compr Physiol 2013; 3:315–330.
43. Corradini E, Pietrangelo A. Iron and steatohepatitis. J Gastroenterol Hepatol 2012; 27(Suppl2): 42–46.
44. Milic S, Mikolasevic I, Orlic L, et al. The role of iron and iron overload in chronic liver disease. Med Sci Monit 2016; 22:2144–2151.
45. Bashir MR, Wolfson T, Gamst AC, et al. Hepatic R2* is more strongly associated with proton density fat fraction than histologic liver iron scores in patients with nonalcoholic fatty liver disease. J Magn Reson Imaging 2019; 49:1456–1466.
46. Armstrong T, Dregely I, Stemmer A, et al. Free-breathing liver fat quantification using a multiecho 3D stack-of-radial technique. Magn Reson Med 2018; 79:370–382.
47. Armstrong T, Ly KV, Murthy S, et al. Free-breathing quantification of hepatic fat in healthy children and children with nonalcoholic fatty liver disease using a multi-echo 3-D stack-of-radial MRI technique. Pediatr Radiol 2018; 48:941–953.
48. Lohöfer FK, Kaissis GA, Müller-Leisse C, et al. Acceleration of chemical shift encoding-based water fat MRI for liver proton density fat fraction and T2* mapping using compressed sensing. PLoS One 2019; 14:e0224988.
49. Mann LW, Higgins DM, Peters CN, et al. Accelerating MR imaging liver steatosis measurement using combined compressed sensing and parallel imaging: A quantitative evaluation. Radiology 2016; 278:247–256.
50. Lustig M, Donoho D, Pauly JM. Sparse MRI The application of compressed sensing for rapid MR imaging. Magn Reson Med 2007; 58:1182–1195.
51. Chappell KE, Patel N, Gatehouse PD, et al. Magnetic resonance imaging of the liver with ultrashort TE (UTE) pulse sequences. J Magn Reson Imaging 2003; 18:709–713.
52. Zhu A, Hernando D, Johnson KM, Reeder SB. Characterizing a short T_2* signal component in the liver using ultrashort TE chemical shift-encoded MRI at 1.5T and 3.0T. Magn Reson Med 2019; 82:2032–2045.
53. Horng DE, Hernando D, Reeder SB. Quantification of liver fat in the presence of iron overload. J Magn Reson Imaging 2017; 45:428–439.
54. Liau J, Shiehmorteza M, Girard OM, Sirlin CB, Bydder M. Evaluation of MRI fat fraction in the liver and spine pre and post SPIO infusion. Magn Reson Imaging 2013; 31:1012–1016.
55. Bashir MR, Zhong X, Nickel MD, et al. Quantification of hepatic steatosis with a multistep adaptive fitting MRI approach: prospective validation against MR spectroscopy. AJR Am J Roentgenol 2015; 204:297–306.
56. Imajo K, Kessoku T, Honda Y, et al. Magnetic resonance imaging more accurately classifies steatosis and fibrosis in

patients with nonalcoholic fatty liver disease than transient elastography. Gastroenterology 2016; 150:626–637.e7.
57. Park CC, Nguyen P, Hernandez C, et al. Magnetic resonance elastography vs transient elastography in detection of fibrosis and noninvasive measurement of steatosis in patients with biopsy-proven nonalcoholic fatty liver disease. Gastroenterology 2017; 152:598–607.e2.
58. Raptopoulos V, Karellas A, Bernstein J, Reale FR, Constantinou C, Zawacki JK. Value of dual-energy CT in differentiating focal fatty infiltration of the liver from low-density masses. AJR Am J Roentgenol 1991; 157:721–725.
59. Hyodo T, Yada N, Hori M, et al. Multimaterial decomposition algorithm for the quantification of liver fat content by using fast-kilovolt-peak switching dual-energy CT: Clinical Evaluation. Radiology 2017; 283:108–118.
60. Roehlen N, Crouchet E, Baumert TF. Liver fibrosis: mechanistic concepts and therapeutic perspectives. Cells 2020; 9:875.
61. Angulo P, Kleiner DE, Dam-Larsen S, et al. Liver fibrosis, but no other histologic features, is associated with long-term outcomes of patients with nonalcoholic fatty liver disease. Gastroenterology 2015; 149:389–397.e10.
62. Ekstedt M, Hagström H, Nasr P, et al. Fibrosis stage is the strongest predictor for disease-specific mortality in NAFLD after up to 33 years of follow-up. Hepatology 2015; 61:1547–1554.
63. Muthupillai R, Lomas DJ, Rossman PJ, Greenleaf JF, Manduca A, Ehman RL. Magnetic resonance elastography by direct visualization of propagating acoustic strain waves. Science 1995; 269:1854–1857.
64. Rouvière O, Yin M, Dresner MA, et al. MR elastography of the liver: preliminary results. Radiology 2006; 240:440–448.
65. Overmoyer BA, McLaren CE, Brittenham GM. Uniformity of liver density and nonheme (storage) iron distribution. Arch Pathol Lab Med 1987; 111:549–554.
66. Cui J, Heba E, Hernandez C, et al. Magnetic resonance elastography is superior to acoustic radiation force impulse for the Diagnosis of fibrosis in patients with biopsy-proven nonalcoholic fatty liver disease: A prospective study. Hepatology 2016; 63:453–461.
67. Singh S, Venkatesh SK, Loomba R, et al. Magnetic resonance elastography for staging liver fibrosis in non-alcoholic fatty liver disease: a diagnostic accuracy systematic review and individual participant data pooled analysis. Eur Radiol 2016; 26:1431–1440.
68. Ichikawa S, Motosugi U, Ichikawa T, et al. Magnetic resonance elastography for staging liver fibrosis in chronic hepatitis C. Magn Reson Med Sci 2012; 11:291–297.
69. Masugi Y, Abe T, Tsujikawa H, et al. Quantitative assessment of liver fibrosis reveals a nonlinear association with fibrosis stage in nonalcoholic fatty liver disease. Hepatol Commun 2018; 2:58–68.
70. Venkatesh SK, Wang G, Lim SG, Wee A. Magnetic resonance elastography for the detection and staging of liver fibrosis in chronic hepatitis B. Eur Radiol 2014; 24:70–78.
71. Singh S, Venkatesh SK, Wang Z, et al. Diagnostic performance of magnetic resonance elastography in staging liver fibrosis: a systematic review and meta-analysis of individual participant data. Clin Gastroenterol Hepatol 2015; 13:440–451.e6.
72. Radiological Society of North America. QIBA Profile: Magnetic Resonance Elastography of the Liver. Stage 2: consensus profile. https://qibawiki.rsna.org/images/a/a5/MRE-QIBAProfile-2018-05-02-CONSENSUS.pdf. (Accessed: Feb 15, 2022)
73. Lee DH, Lee JM, Han JK, Choi BI. MR elastography of healthy liver parenchyma: Normal value and reliability of the liver stiffness value measurement. J Magn Reson Imaging 2013; 38:1215–1223.
74. Motosugi U, Ichikawa T, Amemiya F, et al. Cross-validation of MR elastography and ultrasound transient elastography in liver stiffness measurement: discrepancy in the results of cirrhotic liver. J Magn Reson Imaging 2012; 35:607–610.
75. Yoon JH, Lee JM, Joo I, et al. Hepatic fibrosis: prospective comparison of MR elastography and US shear-wave elastography for evaluation. Radiology 2014; 273:772–782.
76. Toguchi M, Tsurusaki M, Yada N, et al. Magnetic resonance elastography in the assessment of hepatic fibrosis: a study comparing transient elastography and histological data in the same patients. Abdom Radiol (NY) 2017; 42:1659–1666.
77. Morisaka H, Motosugi U, Glaser KJ, et al. Comparison of diagnostic accuracies of two- and three-dimensional MR elastography of the liver. J Magn Reson Imaging 2017; 45:1163–1170.
78. Loomba R, Cui J, Wolfson T, et al. Novel 3D magnetic resonance elastography for the noninvasive diagnosis of advanced fibrosis in NAFLD: A prospective study. Am J Gastroenterol 2016; 111:986–994.
79. Kim DW, Kim SY, Yoon HM, Kim KW, Byun JH. Comparison of technical failure of MR elastography for measuring liver stiffness between gradient-recalled echo and spin-echo echo-planar imaging: A systematic review and meta-analysis. J Magn Reson Imaging 2020; 51:1086–1102.
80. Choi SL, Lee ES, Ko A, et al. Technical success rates and reliability of spin-echo echo-planar imaging (SE-EPI) MR elastography in patients with chronic liver disease or liver cirrhosis. Eur Radiol 2020; 30:1730–1737.
81. Hsu C, Caussy C, Imajo K, et al. Magnetic resonance vs transient elastography analysis of patients with nonalcoholic fatty liver disease: A systematic review and pooled analysis of individual participants. Clin Gastroenterol Hepatol 2019; 17:630–637.e8.
82. Yoon JH, Lee JM, Woo HS, et al. Staging of hepatic fibrosis: comparison of magnetic resonance elastography and shear wave elastography in the same individuals. Korean J Radiol 2013; 14:202–212.
83. Shire NJ, Yin M, Chen J, et al. Test-retest repeatability of MR elastography for noninvasive liver fibrosis assessment in hepatitis C. J Magn Reson Imaging 2011; 34:947–955.
84. Trout AT, Serai S, Mahley AD, et al. Liver stiffness measurements with MR elastography: Agreement and repeatability across imaging systems, field strengths, and pulse sequences. Radiology 2016; 281:793–804.
85. Taouli B, Tolia AJ, Losada M, et al. Diffusion-weighted MRI for quantification of liver fibrosis: preliminary experience. AJR Am J Roentgenol 2007; 189:799–806.
86. Wang Y, Ganger DR, Levitsky J, et al. Assessment of chronic hepatitis and fibrosis: comparison of MR elastography and diffusion-weighted imaging. AJR Am J Roentgenol 2011; 196:553–561.

87. Jang W, Jo S, Song JS, Hwang HP, Kim SH. Comparison of diffusion-weighted imaging and MR elastography in staging liver fibrosis: a meta-analysis. Abdom Radiol (NY) 2021; 46:3889–3907.
88. Le Bihan D, Breton E, Lallemand D, Grenier P, Cabanis E, Laval-Jeantet M. MR imaging of intravoxel incoherent motions: application to diffusion and perfusion in neurologic disorders. Radiology 1986; 161:401–407.
89. Fu F, Li X, Chen C, et al. Non-invasive assessment of hepatic fibrosis: comparison of MR elastography to transient elastography and intravoxel incoherent motion diffusion-weighted MRI. Abdom Radiol (NY) 2020; 45:73–82.
90. Ichikawa S, Motosugi U, Morisaka H, et al. MRI-based staging of hepatic fibrosis: Comparison of intravoxel incoherent motion diffusion-weighted imaging with magnetic resonance elastography. J Magn Reson Imaging 2015; 42:204–210.
91. Kromrey ML, Le Bihan D, Ichikawa S, Motosugi U. Diffusion-weighted MRI-based virtual elastography for the assessment of liver fibrosis. Radiology 2020; 295:127–135.
92. Le Bihan D, Ichikawa S, Motosugi U. Diffusion and intravoxel incoherent motion MR imaging-based virtual elastography: A hypothesis-generating study in the liver. Radiology 2017; 285:609–619.
93. Obmann VC, Berzigotti A, Catucci D, et al. T1 mapping of the liver and the spleen in patients with liver fibrosis-does normalization to the blood pool increase the predictive value? Eur Radiol 2021; 31:4308–4318.
94. Suyama Y, Tomita K, Soga S, et al. T1 magnetic resonance imaging value as a potential marker to assess the severity of liver fibrosis: A pilot study. Eur J Radiol Open 2021; 8:100321.
95. Day CP, James OF. Steatohepatitis: a tale of two "hits"? Gastroenterology 1998; 114:842–845.
96. Tilg H, Moschen AR. Evolution of inflammation in nonalcoholic fatty liver disease: the multiple parallel hits hypothesis. Hepatology 2010; 52:1836–1846.
97. Li X, Wang H. Multiple organs involved in the pathogenesis of non-alcoholic fatty liver disease. Cell Biosci 2020; 10:140.
98. Shi Y, Guo Q, Xia F, et al. MR elastography for the assessment of hepatic fibrosis in patients with chronic hepatitis B infection: does histologic necroinflammation influence the measurement of hepatic stiffness? Radiology 2014; 273:88–98.
99. Ichikawa S, Motosugi U, Nakazawa T, et al. Hepatitis activity should be considered a confounder of liver stiffness measured with MR elastography. J Magn Reson Imaging 2015; 41:1203–1208.
100. Asbach P, Klatt D, Hamhaber U, et al. Assessment of liver viscoelasticity using multifrequency MR elastography. Magn Reson Med 2008; 60:373–379.
101. Deffieux T, Montaldo G, Tanter M, Fink M. Shear wave spectroscopy for in vivo quantification of human soft tissues visco-elasticity. IEEE Trans Med Imaging 2009; 28:313–322.
102. Kruse SA, Smith JA, Lawrence AJ, et al. Tissue characterization using magnetic resonance elastography: preliminary results. Phys Med Biol 2000; 45:1579–1590.
103. Yin M, Glaser KJ, Manduca A, et al. Distinguishing between hepatic inflammation and fibrosis with MR elastography. Radiology 2017; 284:694–705.
104. Sofue K, Onoda M, Tsurusaki M, et al. Dual-frequency MR elastography to differentiate between inflammation and fibrosis of the liver: Comparison with histopathology. J Magn Reson Imaging 2020; 51:1053–1064.
105. Shi Y, Qi YF, Lan GY, et al. Three-dimensional MR elastography depicts liver inflammation, fibrosis, and portal hypertension in chronic hepatitis B or C. Radiology 2021; 301:154–162.
106. Fujimoto K, Tonan T, Azuma S, et al. Evaluation of the mean and entropy of apparent diffusion coefficient values in chronic hepatitis C: correlation with pathologic fibrosis stage and inflammatory activity grade. Radiology 2011; 258:739–748.
107. Taouli B, Chouli M, Martin AJ, Qayyum A, Coakley FV, Vilgrain V. Chronic hepatitis: role of diffusion-weighted imaging and diffusion tensor imaging for the diagnosis of liver fibrosis and inflammation. J Magn Reson Imaging 2008; 28:89–95.
108. França M, Martí-Bonmatí L, Alberich-Bayarri Á, et al. Evaluation of fibrosis and inflammation in diffuse liver diseases using intravoxel incoherent motion diffusion-weighted MR imaging. Abdom Radiol (NY) 2017; 42:468–477.
109. Tosun M, Onal T, Uslu H, Alparslan B, Çetin Akhan S. Intravoxel incoherent motion imaging for diagnosing and staging the liver fibrosis and inflammation. Abdom Radiol (NY) 2020; 45:15–23.
110. Hoad CL, Palaniyappan N, Kaye P, et al. A study of T_1 relaxation time as a measure of liver fibrosis and the influence of confounding histological factors. NMR Biomed 2015; 28:706–714.
111. Hueper K, Lang H, Hartleben B, et al. Assessment of liver ischemia reperfusion injury in mice using hepatic T_2 mapping: Comparison with histopathology. J Magn Reson Imaging 2018; 48:1586–1594.
112. Song J, Yu X, Song W, et al. MRI-based radiomics models developed with features of the whole liver and right liver lobe: Assessment of hepatic inflammatory activity in chronic hepatic disease. J Magn Reson Imaging 2020; 52:1668–1678.